International Journal of Thermophysics, Vol. 27, No. 1, January 2006 (© 2006)
DOI: 10.1007/s10765-006-0024-7

An Experimental Study on Thermal and Electrical Properties of Packed Carbon Nanofibers[1]

H. Xie,[2] H. Gu,[2] M. Fujii,[2] and X. Zhang[2,3]

In the present study, the thermal and electrical properties of packed carbon nanofibers (P-CNFs) have been investigated. A short-hot-wire (SHW) technique was applied to determine simultaneously the thermal conductivity and thermal diffusivity of P-CNFs. In SHW measurements, a platinum wire coated with an alumina layer served as both the heating source and the thermometric sensor. A curve fitting method by matching the experimental data and numerical simulated values was proposed for determining the thermal conductivity and thermal diffusivity of P-CNFs with different packed densities. The electrical conductivities were measured by a four-terminal method where a special vessel with electrodes with circular plates was used. The results indicated that the electrical conductivity increases linearly with an increase in packed density. The thermal conductivity and thermal diffusivity also increase with an increase in packed density. The relation between the thermal conductivity and the electrical conductivity has been shown to be approximately linear. The SHW technique combined with the curve fitting method would be applicable to many kinds of materials.

KEY WORDS: electrical conductivity; packed carbon nanofiber; short-hot-wire; thermal conductivity; thermal diffusivity.

1. INTRODUCTION

Carbon fibers have been attracting increasing interest because they have excellent mechanical properties such as high tensile strength and high

[1] Paper presented at the Seventh Asian Thermophysical Properties Conference, August 23–28, 2004, Hefei and Huangshan, Anhui, P. R. China.

[2] Institute for Materials Chemistry and Engineering, Kyushu University, Kasuga 816-8580, Japan.

[3] To whom correspondence should be addressed. E-mail: xzhang@cm.kyushu-u.ac.jp

elastic modulus, and also have attractive thermal and electrical properties. Although carbon fibers have numerous applications in the fabrication of high performance composite materials, it is very important to know the physical properties of the fibers. For a fiber with a diameter of 10 μm or less, the mechanical and electrical characteristics have been studied often. Also, the thermal characteristics, especially the thermal conductivity, have been obtained from measurements of a composite specimen, including a bundle of the fibers. Recently, Zhang et al. [1, 2] have successfully measured the thermal conductivity of a single free-standing carbon fiber by using a steady-state short-hot-wire method. Due to their small size and excellent properties, carbon nanofibers (CNFs) have great potential for small size devices, e.g., nanoscale electronic devices [3]. Unfortunately, it is very difficult to measure the thermal conductivity of a CNF due to its small size.

The transient short-hot-wire (SHW) method has been successfully used to measure the thermal conductivity and thermal diffusivity of various fluids, molten polymers, and even molten carbonates [4–6]. In the previously used SHW method, the thermal conductivity and thermal diffusivity have been determined from the coefficients of the linear relation between the wire temperature increase and the logarithmic time. This linear relationship implies that in the measuring period the effects of the heat capacity of the hot wire and coating and the heat loss through the electric terminal are negligible. The thermophysical properties of the test sample must fall into the appropriate range. Most kinds of liquids, like water, toluene, glycol, etc., have properties that are consistent with this range. However, for some other materials with a low thermal conductivity or thermal diffusivity, the linear relationship between the wire temperature increase and the logarithmic time does not exist. Then, it is impossible to determine their thermal conductivity and thermal diffusivity through the normal procedure. Therefore, in this case, a curve fitting method by matching the experimental data and numerical simulated values over the complete time range should be applied for extracting the thermal conductivity and thermal diffusivity.

Here, we use the SHW method to measure the thermal conductivity and thermal diffusivity of CNF powders with different packed densities. The corresponding electrical conductivity is also measured with a four-terminal method. The relations between the thermal conductivity and packed density, between the thermal diffusivity and packed density, between the electrical conductivity and packed density, and between the thermal conductivity and the electrical conductivity are investigated.

2. PRINCIPLE OF MEASUREMENTS

The measuring principle of the short-hot-wire technique is similar to that of the normal hot-wire technique [7]. According to the experimental setup used here as described in Section 3.1, the hot-wire probe is immersed in an isotropic medium and initially kept at equilibrium with the medium. The probe is subjected at time $t=0$ to a step change in the voltage applied to the wire. Following this applied voltage, the wire represents a cylindrical heat source with a constant magnitude, q, per unit volume and the temporal evolution of the temperature of the wire is determined by the thermophysical properties of the probe and the test medium. Figure 1 shows the physical model and the coordinate system. In this two-dimensional heat conduction system which is symmetric with respect to the z-axis, the governing equations are non-dimensionalized as follows.

For the hot wire,

$$\frac{\partial \theta_{\mathrm{h}}}{\partial Fo}=\frac{1}{R_{\mathrm{d1}}}\left(\frac{\partial^2 \theta_{\mathrm{h}}}{\partial R^2}+\frac{1}{R}\frac{\partial \theta_{\mathrm{h}}}{\partial R}+\frac{\partial^2 \theta_{\mathrm{h}}}{\partial Z^2}\right)+\frac{R_{\mathrm{c1}}}{R_{\mathrm{d1}}} \tag{1a}$$

For the insulation layer,

$$\frac{\partial \theta_{\mathrm{i}}}{\partial Fo}=\frac{1}{R_{\mathrm{d2}}}\left(\frac{\partial^2 \theta_{\mathrm{i}}}{\partial R^2}+\frac{1}{R}\frac{\partial \theta_{\mathrm{i}}}{\partial R}+\frac{\partial^2 \theta_{\mathrm{i}}}{\partial Z^2}\right) \tag{1b}$$

For the sample,

$$\frac{\partial \theta_{\mathrm{f}}}{\partial Fo}=\frac{\partial^2 \theta_{\mathrm{f}}}{\partial R^2}+\frac{1}{R}\frac{\partial \theta_{\mathrm{f}}}{\partial R}+\frac{\partial^2 \theta_{\mathrm{f}}}{\partial Z^2} \tag{1c}$$

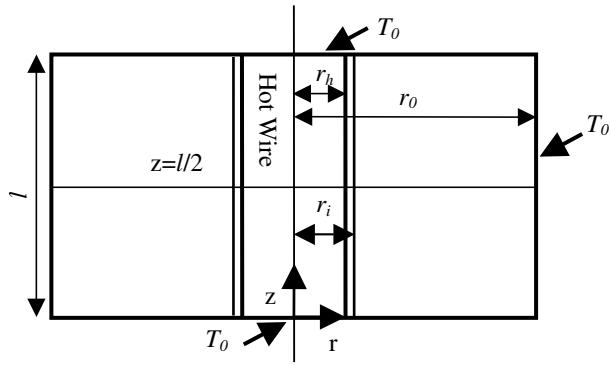

Fig. 1. Physical model of short-hot-wire (SHW) method.

where θ, R, and Z are the dimensionless temperature and radial and longitudinal coordinates, respectively, and Fo is the Fourier number. These dimensionless parameters are defined as

$$\theta = \frac{T - T_0}{\frac{q_v r_h^2}{\lambda_f}}, \quad R = \frac{r}{r_h}, \quad Z = \frac{z}{r_h}, \quad Fo = \frac{\alpha_f t}{r_h^2} \tag{1d}$$

The parameters R_{c1}, R_{d1}, R_{d2}, and those appearing in the boundary conditions are the thermal conductivity and thermal diffusivity ratios of the corresponding layers and are defined as

$$R_{d1} = \frac{\alpha_f}{\alpha_h}, \quad R_{c1} = \frac{\lambda_f}{\lambda_h}, \quad R_{d2} = \frac{\alpha_f}{\alpha_i}, \quad R_{c2} = \frac{\lambda_i}{\lambda_h}, \quad R_{c3} = \frac{\lambda_f}{\lambda_i} \tag{1e}$$

where λ and α are the thermal conductivity and the thermal diffusivity, respectively. In these equations the subscripts h, i, and f denote the short hot wire, the insulation layer, and the test sample, respectively.

The equations are numerically solved by the finite difference method with an alternating direction implicit (ADI) method, under relevant initial and boundary conditions including the continuity conditions for temperature and heat flux at the interfaces between the hot wire and the insulation coating and between the coating and the sample.

In the measurements with the SHW, the volume-averaged temperature is obtained. To correlate the calculated value with experimental results, we analyze the dimensionless volume-averaged hot wire temperature θ_V as a function of the dimensionless heating time Fo. Here θ_V is expressed as

$$\theta_V = \frac{2}{L} \int_0^L \int_0^1 R\theta \, dR \, dZ \tag{2}$$

In Eqs. (1) and (2), the evolution of θ_v is related to the dimensionless parameters in Eq. (1e). For a short hot wire with known thermophysical properties, θ_v depends strongly on the thermophysical properties of the tested sample. To elucidate this dependence, let us investigate the histories of a short hot wire θ_v when testing different samples with relative high and low thermal conductivities, respectively. Figures 2 and 3 show θ_v as a function of $\ln Fo$. In the calculations, the hot wire was taken as a platinum wire with an aspect ratio $L(l/2r_h)$ of 200 and the insulation coating was taken as an alumina layer with a dimensionless thickness of 0.04. The thermal conductivity and the thermal diffusivity of the platinum wire were taken as $71.4\,W{\cdot}m^{-1}{\cdot}K^{-1}$ and $25.2{\times}10^{-6}\,m^2{\cdot}s^{-1}$. The thermal conductivity and thermal diffusivity of the alumina layer

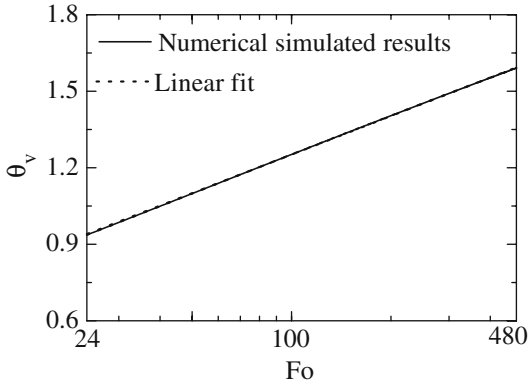

Fig. 2. Linear dependence of θ_v and ln *Fo*.

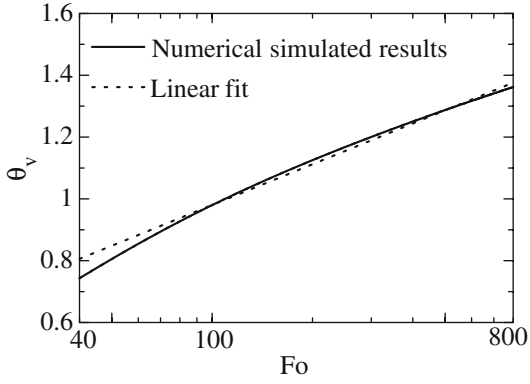

Fig. 3. Nonlinear dependence of θ_v and ln *Fo*.

were taken as $36.0\,W{\cdot}m^{-1}{\cdot}K^{-1}$ and $11.89\times10^{-6}\,m^2{\cdot}s^{-1}$, respectively. For Fig. 2, the thermal conductivity and thermal diffusivity of the assumed sample are $0.6104\,W{\cdot}m^{-1}{\cdot}K^{-1}$ and $0.1466\times10^{-6}\,m^2{\cdot}s^{-1}$, respectively (the values for water at room temperature). For Fig. 3, the thermal conductivity and thermal diffusivity of the supposed sample are $0.05\,W{\cdot}m^{-1}{\cdot}K^{-1}$ and $0.25\times10^{-6}m^2{\cdot}s^{-1}$, respectively. It is clearly shown in Fig. 2 that in the Fourier number range of 24–480, which corresponds to the real experimental time from 0.1 to 2 s, θ_v is linearly dependent on ln(*Fo*). In this case, the result enables us to correlate the θ_v and ln(*Fo*) with a linear equation. For these kinds of samples, the experimental wire temperature rise also increases linearly with the logarithmic time in the above mentioned time range. As reported previously [4–6], the thermal conductivity and thermal

diffusivity are determined by correlating the slope and intercept of the experimental line with those of the calculated line. However, for samples with a low thermal conductivity, the calculated dimensionless temperature rise increases nonlinearly with the logarithmic Fourier number (Fig. 3). The previously used procedure to determine the thermal conductivity and thermal diffusivity by the slope and intercept of the experimental line and of the calculated line could not be used. Therefore, in the present work, a nonlinear curve fitting method by matching the experimental data and numerical simulated values was proposed for extracting the thermal conductivity and thermal diffusivity. This least-squares fit is performed using a downhill simplex method, and the thermal conductivity and the thermal diffusivity are set as free fitting parameters to minimize the square variance between the measured and the calculated temperature rise. As a measure of the reliability of the fit, the square variance, S, of the fit is calculated as

$$S = \sum_{i=1}^{N} \left(T_i^m - T_i^f \right)^2 \tag{3}$$

where T_i^m and T_i^f are the measured and fitted temperature rises, respectively. N is the experimental number of data. A smaller variance represents a higher quality of the fit.

3. EXPERIMENTAL

3.1. Hot-Wire Cell

Figure 4 shows the SHW cell used in these measurements. A short platinum (Pt) wire is welded at both ends to Pt lead wires of 1.5 mm in diameter. The length and diameter of the wire were determined as 8.8 mm and 48 μm from calibration using distilled water and toluene as standard samples. After calibration, the bare probe was coated with a thin alumina layer for insulation by using a sputtering apparatus. The detailed setup of the sputtering device and the coating process have been described in Ref. 8. The thickness of the insulation coating was determined as 0.7 μm from calibration once again by using the same standard samples. The measurements of the thermal conductivity and the thermal diffusivity of CNFs were carried out in vacuum. CNF powders were placed in the cell. The packed density of CNFs was changed by applying different pressures on the piston. To make the packed CNF powders homogeneous, the cell with the CNF sample was subjected to sonication after the piston was fixed.

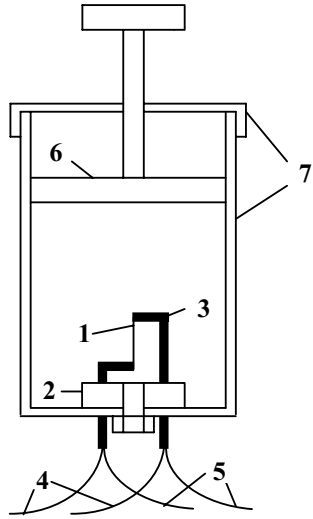

Fig. 4. Schematic diagram of SHW cell: 1 – Pt wire; 2 – Teflon plate; 3 – Pt holders; 4 – lead wires for voltage measurement; 5 – lead wires for heating; 6 – piston; 7 – test vessel.

3.2. Measurement System

A block diagram of the measurement system is shown in Fig. 5. The system consists of a dc power supply and voltage and current measuring and control systems, that is, digital multimeters (Keithley 2002), a personal computer (PC), and PI/O controllers. The heating and measuring systems are controlled by the PC through a GPIB board. The voltage changes of R_{probe}, from which the wire temperature rise can be calculated, are collected and transferred to the PC.

3.3. Four-Terminal Test Vessel

A schematic diagram of the four-terminal test vessel for measuring the electrical conductivity of P-CNFs is presented in Fig. 6. Two cylindrical copper electrodes are fixed on the vessel bottom and on the Teflon piston. Each electrode is connected with two copper lead wires and the four lead wires are connected to the terminals of two multimeters (Keithley 2002). The tested CNF powders are packed in the test vessel. As mentioned in Section 3.1, the packed density of the CNFs was changed

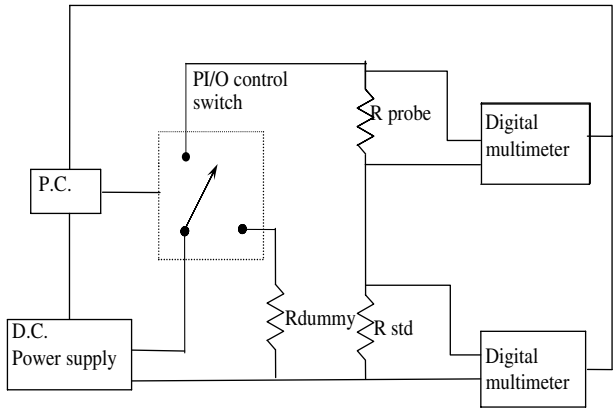

Fig. 5. Schematic diagram of the measurement system.

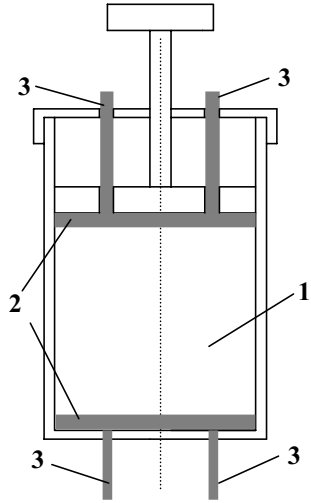

Fig. 6. Schematic drawing of four-terminal test vessel: 1 – Test vessel; 2 – copper electrodes; 3 – leads for measurements.

by applying different pressures on the piston. To make the packed CNF powders homogeneous, the vessel with the CNF sample was subjected to sonication after the piston was fixed.

4. RESULTS AND DISCUSSION

Figure 7 is a micrograph of as-used CNFs, which was taken using a Hitachi S-2460N scanning electron microscope (SEM). These CNFs were supplied by Showa Denko Corp.. Their average diameter and length are 150 nm and 15 μm, respectively. The CNFs were produced by the gas phase method and have good crystallinity. The size and crystallinity were characterized by the supplier and were given in the specifications. It is expected that the CNFs have high electrical and thermal conductivities. However, as shown in Fig. 7, the CNFs are disordered and loose, even after pressing. The porosity is very high, which ranges from 94.7% to 97.8% in the present experiments if the density of the CNFs is taken as 2250 $\mathrm{kg \cdot m^{-3}}$. We cannot expect the thermal and electrical properties of these CNF packed powders to be so high.

The electrical conductivities of P-CNFs as a function of the packed density are presented in Fig. 8. As the CNF powders become denser, the electrical conductivity increases approximately linearly with the packed density. In our measurement density range, the dependence of the electrical conductivity on the packed density is fitted with the following equation:

$$\sigma = 0.0152\rho - 0.7755 \tag{4}$$

where σ is the electrical conductivity and ρ is the packing density of CNFs.

Figure 9 depicts the experimental Pt wire temperature rise with the corresponding best-fit curve for a CNF sample at a density of 120 $\mathrm{kg \cdot^{-3}}$.

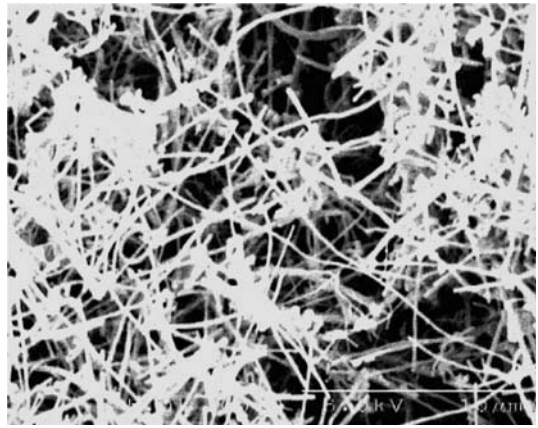

Fig. 7. Micrograph of CNFs.

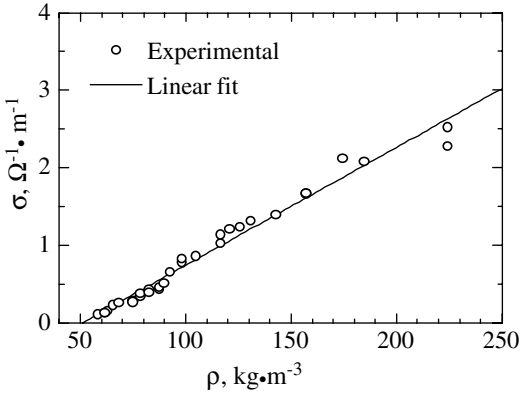

Fig. 8. Dependence of electrical conductivity on packed density.

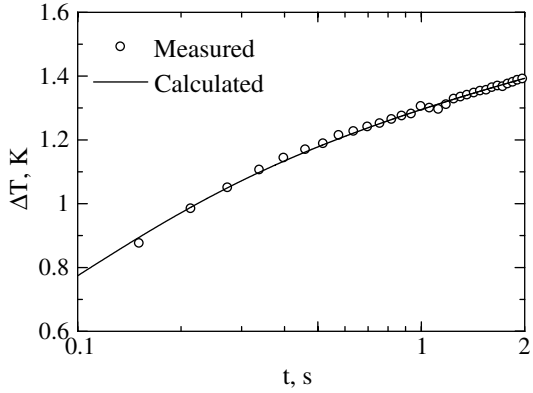

Fig. 9. Measured and simulated results.

The best estimates are: $\lambda = 0.028$ W·m^{-1}·K^{-1} and $\alpha = 0.25 \times 10^{-6}$ m^2·s^{-1}, with a minimum variance. Because the measurements were performed under vacuum, no natural convection took place. The experimental and fitted results are clearly in excellent agreement over the time range from 0.1 to 2 s. The consistency of the experiments and the numerical simulation undoubtedly demonstrated that the true values of the thermal conductivity and thermal diffusivity are essentially the same as the estimates.

For the measurements with a linear relation between the temperature rise and the logarithmic time, the relative errors of the thermal conductivity and thermal diffusivity have been evaluated elsewhere [8]. For the

measurements with a nonlinear relation between the temperature rise and the logarithmic time, the thermal conductivity and thermal diffusivity are determined by a best fit of the experimental data with the calculated temperature rises. The error of this method comes from the measurement as well as the calculation and fit. The relative errors of the thermal conductivity and thermal diffusivity are estimated as

$$\frac{\delta\lambda}{\lambda}=\left[\left(\frac{\delta V}{V}\right)^2+\left(\frac{\delta I}{I}\right)^2+\left(\frac{\delta l}{l}\right)^2+(\delta f_\lambda)^2\right]^{1/2} \tag{5a}$$

$$\frac{\delta\alpha}{\alpha}=\left[\left(\frac{2\delta r_i}{r_i}\right)^2+(\delta f_\alpha)^2\right]^{1/2} \tag{5b}$$

where δf_λ and δf_α are fit errors for λ and α, respectively. l and r_i are determined from calibration using water and toluene with known thermophysical properties, and their relative errors are estimated as [8]

$$\frac{\delta l}{l}=\left[\left(\frac{\delta V}{V}\right)^2+\left(\frac{\delta I}{I}\right)^2+\left(\frac{\delta A}{A}\right)^2+\left(\frac{\delta a}{a}\right)^2+\left(\frac{\delta\lambda_s}{\lambda_s}\right)^2\right]^{1/2} \tag{6a}$$

$$\frac{\delta r_{\mathrm{i}}}{r_{\mathrm{i}}}=\left\{\left[\frac{1}{2}\delta\left(\frac{B}{A}\right)\right]^2+\left[\frac{1}{2}\delta\left(\frac{b}{a}\right)\right]^2+\left(\frac{\delta\alpha_s}{\alpha_s}\right)^2\right\}^{1/2} \tag{6b}$$

Substituting Eqs. (6a) and (6b) into Eqs. (5a) and (5b), we have

$$\frac{\delta\lambda}{\lambda}=\left[2\left(\frac{\delta V}{V}\right)^2+2\left(\frac{\delta I}{I}\right)^2+\left(\frac{\delta A}{A}\right)^2+\left(\frac{\delta a}{a}\right)^2+\left(\frac{\delta\lambda_s}{\lambda_s}\right)^2+(\delta f_\lambda)^2\right]^{1/2} \tag{7a}$$

$$\frac{\delta\alpha}{\alpha}=\left\{\left[\delta\left(\frac{B}{A}\right)\right]^2+\left[\delta\left(\frac{b}{a}\right)\right]^2+\left(\frac{\delta\alpha_s}{\alpha_s}\right)^2+(\delta f_\alpha)^2\right\}^{1/2} \tag{7b}$$

An uncertainty of 1.0% is successfully obtained for a best fit of the thermal conductivity. For thermal diffusivity, the best-fit uncertainty is estimated to be 5.0%. Other error terms have been evaluated previously [8]. From Eqs. (7a) and (7b), the total errors of the measurement are estimated to be 2% for the thermal conductivity and 7% for the thermal diffusivity, respectively.

Figures 10 and 11 show the dependences of the thermal conductivity and thermal diffusivity of P-CNFs on the packed density, respectively. As expected, when the density increases, i.e., when the porosity decreases, the thermal conductivity and thermal diffusivity increase almost linearly. In our measurement density range, the relations between the thermal conductivity and the density is fitted with an expression as

$$\lambda = 0.000385\rho - 0.0188 \tag{8}$$

The linear fitting expression for the thermal diffusivity in the present density range is

$$\alpha = 3.25 \times 10^{-9}\rho - 1.36 \times 10^{-7} \tag{9}$$

As shown in Figs. 10 and 11, these expressions represent the relationships between the thermal conductivity and the packed density and between the thermal diffusivity and the packed density fairly well.

We show the relation between the thermal conductivity and the electrical conductivity in Fig. 12. At the measured packed densities, there is a linear relation between the thermal conductivity and the electrical conductivity. For graphitized pitch-based micro-carbon fiber, Zhang et al. [2] reported a linear relationship between the thermal conductivity and the electrical conductivity. The as-used P-CNFs also show a linear dependence between these two transport properties. However, the electrical conductivities of the P-CNFs are very small, which are less than 1 $\Omega^{-1}\cdot m^{-1}$, while that of a single standing fiber might be as large as 0.6 $M\Omega^{-1}\cdot m^{-1}$.

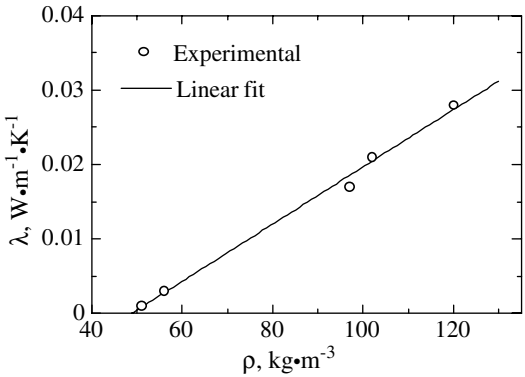

Fig. 10. Thermal conductivity as a function of the packed density.

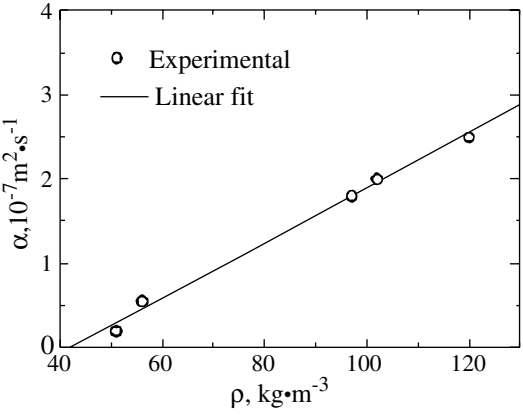

Fig. 11. Dependence of the thermal diffusivity on the packed density.

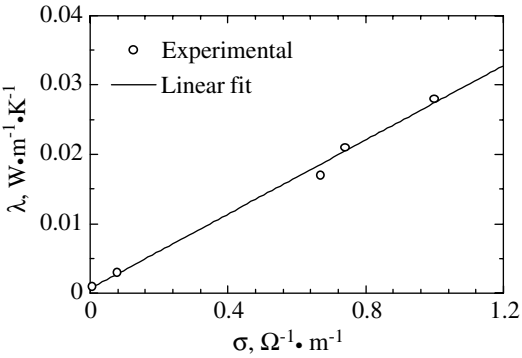

Fig. 12. Relation between the thermal conductivity and electrical conductivity.

5. CONCLUSIONS

The short-hot-wire technique was successfully used to simultaneously determine the thermal conductivities and thermal diffusivities of P-CNFs of different packed densities, by fitting the dependence of the measured wire temperature rise on the logarithmic time to that of the calculated values. The electrical properties of P-CNFs were also measured using a four-terminal method. In the measured density range, the electrical conductivity increases linearly with an increase in packed density. The

thermal conductivity and thermal diffusivity also increase with an increase in packed density. The relation between the thermal conductivity and electrical conductivity has been shown to be approximately linear.

REFERENCES

1. X. Zhang, S. Fujiwara, and M. Fujii, *Int. J. Thermophys.* **21**:965 (2000).
2. X. Zhang, M. Fujii, H. Sakai, H. Xie, and I. Mochida, *Proc. 3rd Int. Conf. on Heat Transfer, Fluid Mechanics, and Thermodynamics*, Cape Town, South Africa (2004), CD-ROM/ZX1.
3. X. Yang, M. A. Guillorn, D. Austin, A. V. Melechko, H. Cui, H. M. Meyer III, V. I. Merkulov, J. B. O. Caughman, D. H. Lowndes, and M. L. Simpson, *Nano Letters* **3**:1751 (2003).
4. M. Fujii, X. Zhang, N. Imaishi, S. Fujiwara, and T. Sakamoto, *Int. J. Thermophys.* **18**:327 (1997).
5. X. Zhang and M. Fujii, *Polymer Eng. Sci.* **43**:1755 (2003).
6. X. Zhang, H. Wicaksono, S. Fujiwara, and M. Fujii, *High Temps.–High Press.* **34**:617 (2002).
7. Y. Nagasaka and A. Nagashima, *Rev. Sci. Instrum.* **52**:229 (1980).
8. X. Zhang and M. Fujii, *Int. J. Thermophys.* **21**:71 (2000).